4*f*-3*d* emission spectra of the rare earths: An interpretation of the lines observed on both sides of the resonances

C. Bonnelle* and P. Motais
Laboratoire de Chimie Physique Matière et Rayonnement, UMR-CNRS 7614, Université Pierre et Marie Curie, 11 rue Pierre et Marie Curie, 75231 Paris cedex 05, France
(Received 30 November 2005; published 27 April 2006)

A general model using a multiconfiguration Dirac-Fock program with Breit interaction and QED corrections is established to calculate the 4*f* core-level transitions in the rare earths. This model is tested by comparing the calculated spectra to the experimental spectra of all the elements of the rare-earth series obtained by electron-induced x-ray emission spectroscopy. Agreement between the *ab initio* energies calculated in the free-ion model and the energies measured for the solid rare-earth spectra is of the order of 1 to 2 eV, i.e., better than 0.2%. Each observed structure is interpreted. Variation of the intensity ratios of the various emissions along the lanthanide series is explained. These results prove the validity of our theoretical model to describe the 4*f*-3*d* transitions in the solids. This general model can be used to interpret the 4*f* core-level transitions observed from other spectroscopies.

DOI: 10.1103/PhysRevA.73.042504 PACS number(s): 32.30.Rj, 78.70.En, 34.80.Dp

I. INTRODUCTION

Most of the physical properties of the rare earths are related to the presence of the 4*f* electronic subshell which fills up progressively along the series. The 4*f* ionization energies are comparable in these elements to those of the 5*d* and 6*s* valence electrons. However, the spatial extension of the 4*f* subshell is small and it remains inside the 5*s* and 5*p* subshells. Consequently the 4*f* electrons do not participate in the chemical bonding and retain an atomic character in the solids while the 5*d* and 6*s* valence electrons are hybridized with the ligand orbitals in the compounds and supply the chemical binding. The rare earths are generally trivalent and their configuration is designated by $4f^m(5d+6s)^3$. Exceptions exist in some cases, e.g., for metallic Eu and Yb, which have two valence electrons and the $4f^m(5d+6s)^2$ configuration, and for some Ce, Sm, Eu, Tb, Tm, and Yb compounds.

The x-ray spectra of the rare earths show pronounced structures due to the presence of the 4*f* open subshell. These spectra depend on the electronic configuration and can be used to determine the number of 4*f* electrons in the rare-earth compounds. This is of great interest in the determination of the physical properties of the solids, in particular in the case of intermediate valence compounds.

In electron-induced x-ray emission spectroscopy (EXES), and in a general point of view for systems interacting in collisional processes, excitation to localized states and ionization to continuum states can take place simultaneously. Consequently, excitation and ionization spectra are obtained. Their relative intensities can be measured and the probabilities of the excitation and ionization processes deduced from these measurements. In a solid, excited states with a core hole can be created simultaneously with the ionized states only if one of the elements present in the material has a localized open subshell. This is the case for the rare earths and the actinides.

The *nd* (with $n=3,4$) spectra of the rare earths have a particular interest because they involve the electric dipolar transitions between the *nd* and 4*f* subshells. Comparison between the 3*d*-4*f* absorption and emission spectra has shown that both these types of transitions are located in the same energy range [1,2]. The structures observed in the emission spectra were then considered as a consequence of the self-absorption of the emitted radiation in the target. Subsequently, experiments using a probe electron beam of energy near the 3*d* excitation threshold revealed that the more intense 3*d* emissions occur at the same energy as the absorption lines [3]. These emissions have been interpreted as the direct decay of the $3d^9 4f^{m+1}$ excited states to the ground state, i.e., as the reverse process of the $3d \rightarrow 4f$ excitation [4]. For this reason, they have been called resonance lines. Their observation in the 3*d* spectra of open *f*-shell elements is an experimental proof of the highly localized character of the 4*f* excited states in the studied material and suggests that the 4*f*-3*d* transitions, like those between the core levels, can be treated by considering the isolated atom or ion.

Further features, present at both lower and higher energies around the resonance lines in the electron-induced rare-earth 3*d* emission spectra, make them clearly more complex than the corresponding absorption spectra. The high-energy emissions were initially attributed to satellites and received little attention. The low-energy emissions were erroneously considered as the $M\alpha$ ($4f$-$3d_{5/2}$) and $M\beta$ ($4f$-$3d_{3/2}$) emissions, i.e., the emissions from the normally occupied 4*f* states in the absence of the core hole, labeled diagram lines [2,5]. Anomalies in the relative intensities of the $3d_{3/2}$ and $3d_{5/2}$ emissions were observed and remained unexplained. Comparisons between the fluorescence and electron-induced spectra had been performed in some cases [5,6] but they have not led to modification of the previous interpretations. Several different types of emissions are present in the rare-earth *nd* spectra. These spectra are thus complex and their

*Electronic address: cbon@ccr.jussieu.fr

interpretation is possible only by comparing them with the predictions of a suitable theoretical model.

In this paper, we apply a relativistic atomic model to calculate the entire energy-level systems of the configurations involved in the $4f$-$3d$ and $5p$-$3d$ transitions of the rare earths. The calculations are performed for all the elements of the series except for Pm. In the middle of the $4f$ shell, they involve up to around 600 000 transitions and have not, to our knowledge, been undertaken before. From comparison between the calculated spectra and the spectral characteristics of the $4f$-$3d$ and $5p$-$3d$ emissions induced by electron impact, a successful interpretation of all the observed features is obtained. Interpretations of the $4f$-$3d$ emissions are given and the variation of the intensity ratios of the $4f$-$3d_{5/2}$ and $4f$-$3d_{3/2}$ emissions along the series is explained. The resonance lines of the metal and the oxide are observed at the same energy if the number of $4f$ electrons is the same in both materials. This confirms that the interactions between the $4f$ and valence electrons is negligible. The theoretical model developed in this work can also be used to interpret the $4f$-$3d$ fluorescence spectra [7–10] as well as the corresponding nonradiative transitions.

II. GENERAL METHODS

With the aim of interpreting the EXE spectra, it is necessary to take into account the specificities of the incident electron beam interaction with the target. An incident electron may lose any part of its energy by exciting or ionizing a core electron, the remaining part being carried out as the kinetic energy of the outgoing electrons [11]. Consequently, both excited and ionized states can be produced under electron impact. The $3d^9 4f^{m+1}$ excited and $3d^9 4f^m$ ionized configurations of the rare earths are created in a ratio depending on the electron cross sections for excitation and ionization. For a given atom, this ratio depends on the energy of the incident electrons. For an incident energy E_0 just above the $3d$ ionization threshold, the excitation is predominant, while for higher E_0 values the ionization is favored.

All the levels of the $3d^9 4f^{m+1}$ configuration can be populated for E_0 near threshold [12]. However, the electronic cross sections corresponding to dipolar electrical transitions from the ground level $3d^{10}4f^m\ ^{2S+1}L_J$ to the excited $3d^9 4f^{m+1} J, J\pm 1$ levels have the highest values and this is enhanced for the heavy rare earths [13]. These excited levels decay to all the allowed levels of the $3d^{10}4f^m$ configuration while the resonance lines correspond only to the transitions to its ground level $^{2S+1}L_J$. Thus, the resonance lines are only a part of the total allowed emissions from the excited $J, J\pm 1$ levels. Additional peaks appear on the low-energy side of each resonance line. We label these lines $J, J\pm 1$ emissions. The ensemble of lines emitted from all the levels of the $3d^9 4f^{m+1}$ excited configuration is labeled excitation emissions. When E_0 exceeds twice the threshold energy, the ionization of a core electron is favored. The time scale of an ionization process is much shorter than the lifetime of the core hole. Consequently, the J levels of the ionized configuration are populated statistically before the core hole decays and transitions from all these levels contribute to the emission spectrum; they are labeled ionization emissions.

The energies and the probabilities of the various electric dipolar $4f$-$3d$ emissions are calculated for each rare earth. From these, we have derived the corresponding spectra of the trivalent rare earths with the same method as in Refs. [14,15]. These spectra are compared to the electron-induced experimental spectra observed for the solid rare earths. The good agreement obtained between the calculated and experimental energies confirms the localized character of the $4f$ electrons as well as our interpretation of the resonance lines and suggests an interpretation of all the remaining observed structures. Large intensity variations of the experimental structures are observed as a function of the incident electron energy E_0. They are discussed by taking into account the excitation and ionization probabilities and the self-absorption.

The $5p$-$3d$ atomic lines fall in the same spectral range as the above transitions. The $5p$-$3d_{5/2}$ lines are located some 15 eV toward the lower energy than the $4f$-$3d_{5/2}$ transitions and are clearly separated from them while the $5p$-$3d_{3/2}$ lines are mixed with them. Two different $5p$-$3d_{5/2}$ type lines have been observed in the rare earths: the diagram emissions in the $3d^9 4f^m$ ion and the emissions in the $3d^9 4f^{m+1}$ excited atom, labeled emissions in the presence of a spectator electron. We have calculated both types of lines by taking into account all the levels of the initial and final configurations. We find that the difference between the $5p$-$3d$ transition probabilities in the ion and the excited atom is small for all rare earths. Consequently, the relative intensities of the $5p$-$3d$ lines enable direct determination of the ratio of the excitation and ionization probabilities in the observation conditions.

III. CALCULATION OF THE EMISSION SPECTRA

By using a multiconfigurational Dirac-Fock (MCDF) program including Breit interaction and QED corrections [16], we have calculated the energies and the probabilities of the radiative transitions from the $3d^9 4f^{m+1}$ excited and $3d^9 4f^m$ ionized configurations to the corresponding $3d^{10}$ final configurations with one f or p missing electron. These *ab initio* calculations are carried out for all the trivalent rare-earth ions from La^{3+} to Yb^{3+}. The initial and final states of the transitions are obtained from the extended average level extension of the MCDF method coupled with the Slater transition state [17]. The velocity form of the transition matrix elements is used. Each group of $3d_{3/2}^{-1}4f^m$ or $3d_{5/2}^{-1}4f^m$, with $2 \leqslant m \leqslant 13$, states spreads over a broad energy range due to the multiplet splitting of the d and f open subshells and to the large Coulomb interaction between the d hole and the f electrons. Corrections due to Breit interactions increase with the state energy. For La^{3+}, they vary between -1.6 and -2.1 and for Yb^{3+} between -3.7 and -4.7 eV. The QED correction increases also along the rare-earth series and remains below $+0.05$ eV. No configuration mixing exists between the one-hole configurations and the final two-hole configurations of the energetically allowed Auger transitions because they are widely separated in energy. Thus no shift due to the coupling between the one- and two-hole states is taken into account [18].

TABLE I. Calculated energies E (eV) and probabilities p (10^{10} s^{-1}) of the $4f$-$3d_{5/2}$ and $4f$-$3d_{3/2}$ emissions: excitation emissions, columns 2–5; ionization emissions, columns 7–10.

	$4f$-$3d_{5/2}$		$4f$-$3d_{3/2}$			$4f$-$3d_{5/2}$		$4f$-$3d_{3/2}$	
	E	p	E	p		E	p	E	p
La f^1	836.6	19.5	853.7	39.6					
Ce f^2	882.8	46.0	901.8	77.0	f^1	887.6	23.4	906.4	51.6
Pr f^3	931.1	82.9	951.3	125.4	f^2	934.4	55.8	955.2	101.0
Nd f^4	980.3	132.2	1002.0	182.6	f^3	983.3	100.4	1005.5	161.6
Sm f^6	1080.0	278.9	1106.0	322.9	f^5	1083.3	237.4	1109.7	309.2
Eu f^7	1131.9	380.1	1160.0	406.5	f^6	1135.3	333.7	1163.0	396.4
Gd f^8	1184.6	503.2	1214.9	499.4	f^7	1187.7	452.2	1218.2	492.8
Tb f^9	1238.3	650.8	1270.9	602.1	f^8	1241.4	595.5	1273.8	598.8
Dy f^{10}	1293.2	823.0	1328.0	713.8	f^9	1295.8	766.1	1331.0	714.9
Ho f^{11}	1348.7	1026.8	1385.8	837.6	f^{10}	1353.1	998.4	1389.7	872.1
Er f^{12}	1405.1	1262.7	1445.3	973.5	f^{11}	1407.9	1196.4	1447.8	978.6
Tm f^{13}	1461.0	1533.2	1503.7	1122.5	f^{12}	1465.2	1464.0	1506.1	1129.7
Yb f^{14}	1520.3	1841.2	1567.0	1285.6	f^{13}	1521.9	1769.4	1567.6	1294.7

The ionization transitions are determined by considering that all the J levels of the ionized configuration are populated statistically and by calculating the energy and the probability of all the allowed electric dipolar lines from these J levels to all the levels of the final configuration. Each line is obtained by folding the calculated probability with a Lorentzian broadening function whose width Γ_J results from the lifetime of the inner hole. The total emission is calculated by taking the weighted sum of all the lines. We have calculated the $\Gamma_{5/2}$ and $\Gamma_{3/2}$ widths for La^{3+} and Yb^{2+}. For the closed-shell Yb^{2+} ion, our values are in agreement with those of Ref. [19]. We use for the $\Gamma_{5/2}$ and $\Gamma_{3/2}$ widths the values 0.8 and 1.3 eV for the light rare earths and 1 and 1.5 eV for the heavy rare earths, respectively.

For the excitation transitions, several calculations are presented. In the first one, we consider only the dipole-allowed $J, J\pm1$ excited states from the ground state, $4f^{m\ 2S+1}L_J$, and the lines corresponding to the recombinations from these excited states to the J ground state. These lines are the $4f$-$3d$ resonance lines because they correspond to the reverse process of photoabsorption. In the second calculation, we consider the $J, J\pm1$ emissions taking place from the previous $J, J\pm1$ excited levels to all the dipole-allowed levels of the final configuration. Finally, all the J levels of the excited configuration are assumed to be statistically populated and the calculations are the same as for ionization; these are the excitation emissions.

The energies of the maxima of the calculated spectra E and the weighted sums of the probabilities p are given in Table I, columns 2–5 for $3d_{5/2}$ and $3d_{3/2}$ excitation emissions and columns 7–10 for $3d_{5/2}$ and $3d_{3/2}$ ionization emissions.

Only for La^{3+} is the $4f$-$3d$ emission spectrum simple. It has three excitation lines, which are resonance lines [20], and no $4f$-$3d$ ionization line is present. For Yb^{3+}, one expects also three excitation lines, only one $3d_{5/2}$ resonance line, and 108 ionization lines. The number of lines increases with m along the series up to the half-filled $4f$ subshell ($m=7$) and decreases beyond. For the $4f$-$3d$ emissions from d^9f^7 and d^9f^8, there are 277 827 lines. Consequently, the multiplet components of the strongly split $4f$-$3d$ emissions spread over an energy range clearly broader than the lifetime width Γ of each J level. The excitation transitions calculated for Pr^{3+}, Eu^{3+}, and Er^{3+}, with Γ equal to 0.1 and 1 eV are plotted in Fig. 1. The lifetime broadening has an influence on the height of the spectrum but does not modify its energy exten-

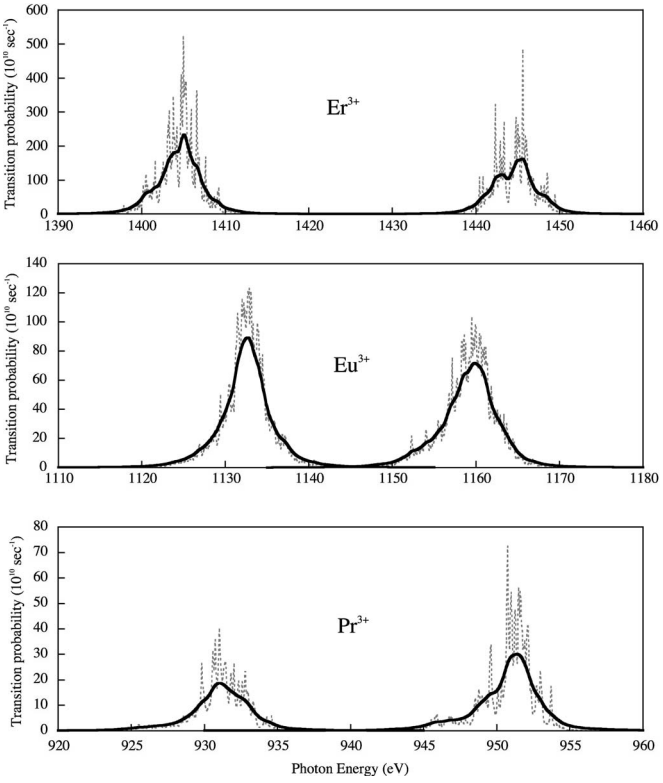

FIG. 1. Excitation emissions of Pr^{3+}, Eu^{3+}, and Er^{3+}: $\Gamma=1$ eV, continuous line; $\Gamma=0.1$ eV, dashed line.

TABLE II. $3d_{5/2}$:$3d_{3/2}$ ratios R: $R1$, resonant lines; $R2$, $J,J\pm1$ emissions; $R3$, excitation emissions; $R4$, ionization emissions.

	$R1$	$R2$	$R3$	$R4$
La f^1	0.49	0.49	0.49	
Ce f^2	0.74	0.61	0.60	0.45
Pr f^3	0.86	0.67	0.66	0.55
Nd f^4	1.09	0.74	0.72	0.62
Sm f^6	1.58	0.90	0.86	0.77
Eu f^7	2.13	1.02	0.94	0.84
Gd f^8	2.00	1.04	1.01	0.92
Tb f^9	2.62	1.08	1.08	0.99
Dy f^{10}	3.80	1.14	1.15	1.07
Ho f^{11}	6.19	1.22	1.23	1.15
Er f^{12}	9.64	1.61	1.30	1.22
Tm f^{13}	20.4	2.30	1.37	1.30
Yb f^{14}			1.43	1.37
Lu f^{14}				1.43

sion. This extension is due to the great number of allowed lines around a few energies.

In our model, the open $4f$ subshell of the rare earths is treated as an atomic subshell. This atomic behavior is responsible for the creation of the $3d^9 4f^{m+1}$ discrete excitation states, their radiative recombination to other excited configurations or to the ground state, and also the radiative recombination from the $3d^9 4f^m$ ionized configuration to the $3d^{10}4f^{m-1}$ final configuration. The additional $4f$ electron of the $3d^9 4f^{m+1}$ excited configuration partially screens the excess of positive nuclear charge induced by the ejection of the $3d$ core electron. Consequently, the average energy of the $3d^9 4f^{m+1}$ excited configuration is lower than that of the $3d^9 4f^m$ ionized configuration. The same holds for the energies of the $5p^5 4f^{m+1}$ and $4f^m$ configurations with respect to the energies of the $5p^5 4f^m$ and $4f^{m-1}$ configurations. From our calculations, the electrostatic interaction between the $4f$ electrons and the $3d$ hole is larger than that between the $4f$ electrons and a $5p$ or $4f$ hole. Consequently, the $4f$-$3d$ and $5p$-$3d$ emissions from the $3d^9 4f^{m+1}$ excited configurations are located toward lower energies with respect to the emissions from the $3d^9 4f^m$ ionized configurations.

The ratios of $4f$-$3d_{5/2}$ to $4f$-$3d_{3/2}$ transitions are given in Table II. The radiative probabilities are calculated for the entire $3d^{-1}4f^{m+1}$ or $3d^{-1}4f^m$ configuration; then the sums of the probabilities are determined for each $3d_{3/2}$ and $3d_{5/2}$ group of lines separately. These sums are obtained by multiplying each probability by the statistical weight of the J level of the involved excited, or ionized, configuration and by normalizing with the sum of the statistical weights of all the levels, in order to take into account the statistical population of the states. It should be noted that the $3d_{5/2}$:$3d_{3/2}$ ratio depends very little on the weighing because of the large number of the emission lines. In column 2 of Table II, we give the ratios for the resonance lines ($R1$), in column 3 for the $J,J\pm1$ lines ($R2$), in column 4 for the excitation lines ($R3$), and in column 5 for the ionization lines ($R4$). These ratios increase along the rare-earth series. For La^{3+}, $R1$, $R2$, and $R3$ have the same value. From this point on, $R1$ varies more rapidly than the others. Differences between the ratios calculated for the $J,J\pm1$ emissions ($R2$) and the excitation emissions ($R3$) become noticeable only for the heavy rare earths from Er on.

Very few calculations for only the more intense lines of two or three rare earths have been reported. They were made for each of the $3d_{3/2}$- and $3d_{5/2}$-based levels separately as well as calculations of the x-ray line energies [18] and of the fluorescence yields [21]. For the excitation emissions, we performed these separate calculations of the transitions involving the $3d_{5/2}^{-1}4f^{m+1}$ from those involving the $3d_{3/2}^{-1}4f^{m+1}$ excited configuration for the entire rare-earth series. The weighted sums of the radiative probabilities from all the J levels of both separate configurations have been determinated and, as above, normalized with the sum of the statistical weights of the $3d^9 4f^{m+1}$ configuration. In contrast with the values given in Table II, the $3d_{5/2}$:$3d_{3/2}$ ratio stays approximately equal to 1.5 for all rare earths.

When both emission groups are calculated together, the probabilities of the $3d_{5/2}$-based transitions decrease and those of the $3d_{3/2}$-based transitions increase, making the $3d_{5/2}$:$3d_{3/2}$ ratio vary with the number of $4f$ electrons. It is approximatively equal to unity for ions having the $4f$ subshell half filled and tends to the value characteristic of the complete $4f$ subshell for Yb^{3+}. This behavior is not due to selection rules, unlike a previous suggestion [22]. The explanation must be searched for in the couplings. Among them, the $3d$-$4f$ electrostatic interactions have an important role as already mentioned above. They partially change the character of the states and are responsible for the tendency of the $4f$ electrons to have preferentially $5/2$ character. Then the transitions connecting these states to $3d_{3/2}$ become more intense than those to $3d_{5/2}$ for the light rare earths and this explains the variation of the $3d_{5/2}$:$3d_{3/2}$ ratio. As a rule, when the initial and final states are strongly split, the relative intensities of the nlj- and $nl(j+1)$-based emissions cannot be deduced from the statistical weights of the two base levels.

Nonradiative decay channels can modify the $3d_{5/2}$:$3d_{3/2}$ ratio [9,20]. For the rare earths, resonant Coster-Kronig transitions from $3d_{3/2}^{-1}4f^{m+1}$ to $3d_{5/2}^{-1}4f^m$ can be energetically possible, particularly in the presence of valence electrons. We have calculated the probabilities of these transitions for some rare earths and found them to be more than one order of magnitude higher than the radiative ones. These transitions decrease the number of excited states with a $3d_{3/2}$ hole and increase that of the ionized states with a $3d_{5/2}$ hole. When the Auger and Coster-Kronig probabilities are taken into account, their combined effect is to increase the $3d_{5/2}$:$3d_{3/2}$ ratio by a factor of 1.2–1.3, except for La^{3+} and Yb^{3+}, for which it is multiplied by about 1.4. As a result, the lifetime of the $3d_{3/2}$ level decreases and its width increases with respect to that of the $3d_{5/2}$ level by about 0.5 eV for the entire series of rare earths. This broadening effect is taken into account in the calculations and has as a consequence the decrease of the relative height of the $3d_{3/2}$-based spectrum with respect to the $3d_{5/2}$ one.

The energies and probabilities of the $5p$-$3d$ emissions have been calculated by including all the J levels of either

TABLE III. Calculated energies E (eV) and probabilities p (10^{10} s^{-1}) of the $5p$-$3d_{5/2}$ and $5p$-$3d_{3/2}$ emissions: emissions in the presence of a $4f$ spectator electron, columns 2–5, diagram emission, columns 7–10.

	$5p$-$3d_{5/2}$		$5p$-$3d_{3/2}$			$5p$-$3d_{5/2}$		$5p$-$3d_{5/2}$	
	E	p	E	p		E	p	E	p
La f^1	813.0	4.80	827.1	3.45	f^0	821.2	5.40	835.2	3.83
Ce f^2	860.0	5.23	875.5	3.79	f^1	867.8	5.85	883.9	4.20
Pr f^3	907.7	5.66	925.1	4.16	f^2	915.4	6.33	932.0	4.59
Nd f^4	956.2	6.12	975.3	4.55	f^3	963.8	6.82	982.6	5.01
Sm f^6	1054.1	7.10	1078.8	5.41	f^5	1061.5	7.87	1085.6	5.92
Eu f^7	1105.8	7.62	1132.2	5.88	f^6	1113.0	8.45	1138.8	6.44
Gd f^8	1158.2	8.15	1186.8	6.38	f^7	1165.4	9.03	1193.6	6.97
Tb f^9	1211.7	8.71	1242.6	6.91	f^8	1218.7	9.64	1249.1	7.53
Dy f^{10}	1267.1	9.28	1298.7	7.45	f^9	1279.0	10.27	1305.4	8.11
Ho f^{11}	1323.2	9.88	1356.6	8.05	f^{10}	1329.3	10.91	1362.9	8.75
Er f^{12}	1378.9	10.52	1415.7	8.69	f^{11}	1386.5	11.59	1421.9	9.43
Tm f^{13}	1437.6	11.18	1476.3	9.37	f^{12}	1442.9	12.31	1482.2	10.16
Yb f^{14}	1495.4	11.87	1536.9	10.10	f^{13}	1500.2	13.06	1542.0	10.93

the excited or the ionized configurations. The $5p$-$3d$ emissions in the presence of the $4f$ spectator electron (Table III, columns 2–5) are located toward the lower energies of the diagram emissions in the ion (columns 7–10) as expected. The separation is about 5–8 eV. The intensities of the $4f$-$3d$ and $5p$-$3d$ emissions increase along the series, more strongly for the $4f$-$3d$ that for the $5p$-$3d$ ones. For the light rare earths, the $4f$-$3d$ emissions are about an order of magnitude stronger than the $5p$-$3d$ emissions.

IV. EXPERIMENT

The spectra reported here were recorded with a beryl curved-crystal monochromator. The resolution of the monochromator is about 0.2 eV at 900 eV and 0.6 eV at 1500 eV. The target is inclined by 45° with respect to the incident electron and emitted photon beams [20]. The spectra were observed for different incident energies of the probe electron beam, E_0, varying from the ionization threshold, E_i, up to 2 or 2.5 times the threshold. The E_i [23] and E_0 energies are given in Table IV. Under our experimental conditions, the self-absorption in the target remains weak except for the resonance lines and for the lines located in the same energy range, which are already clearly self-absorbed from $E_0 = 1.5E_i$. At low values of E_0, the spectra show few structures. When E_0 increases, the number of the features increases due to the self-absorption effect.

For each rare earth, the $4f$-$3d$ emissions from the metal and the stable oxide have been compared. When the valence is the same in the both materials, the energies of the different features are the same. They are independent of the physicochemical characteristics of the target. These observations confirm the strongly localized character of the $4f$ electrons and justify the use of the free-ion model. The valence electrons screen partially the core hole. This screening shifts the binding energies toward lower ones in the solid with respect to the energies calculated in the free ion. This effect must be considered in the comparison between the calculated and experimental spectra.

The excitation lines are slightly more intense for the oxide than for the metal. The explanation is as follows. For a conductor material, the excited states are energetically mixed with extended valence states and tunneling of the excited electron to the extended states is possible. This process decreases the population of the excited states with respect to that of the ionized ones but it does not change their localized character. In the oxides, excited states created by charge transfer from the oxygen valence band to the $4f$ states in the presence of the $3d$ core hole had been expected [24]. If electronic transfer between the valence band and the $4f$ states takes place in the metal [6,25], the energies of the $3d^9 4f^{n+1} V^{-1}$ (V designates the valence electrons) excited states and of their transitions to $3d^{10}$ should be different from

TABLE IV. Energies (eV): $3d_{5/2}$ and $3d_{3/2}$ threshold energies E_i [23], columns 2 and 3; incident energies E_0, columns 4 and 5.

	$Ei(3d_{5/2})$	$E_i(3d_{3/2})$	E_0	E_0
Ce	883.3	901.3	1500	
Pr	931.0	951.1	1100	3000
Nd	977.7	999.9	1200	3000
Sm	1080.2	1106.0	1400	3000
Eu	1130.9	1160.6	1400	2300
Gd	1185.2	1217.2	1400	2250
Tb	1241.2	1275.0	1400	3000
Dy	1294.9	1332.5	1500	2800
Ho	1351.4	1391.5	1500	2800
Er	1409.3	1453.3	1600	2400
Tm	1467.7	1514.6	1600	3000
Yb	1527.8	1576.3	1700	3000

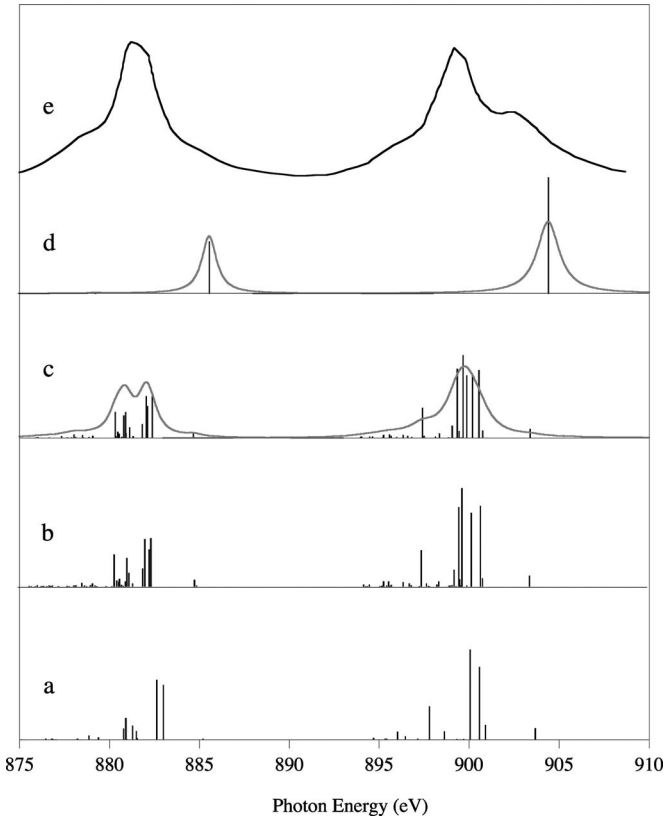

FIG. 2. Ce^{3+} calculated and experimental emissions: (a) resonance lines; (b) $J,J\pm1$ emissions; (c) $4f$-$3d$ excitation emissions; (d) $4f$-$3d$ ionization emissions; (e) metal observed at 1.5 kV.

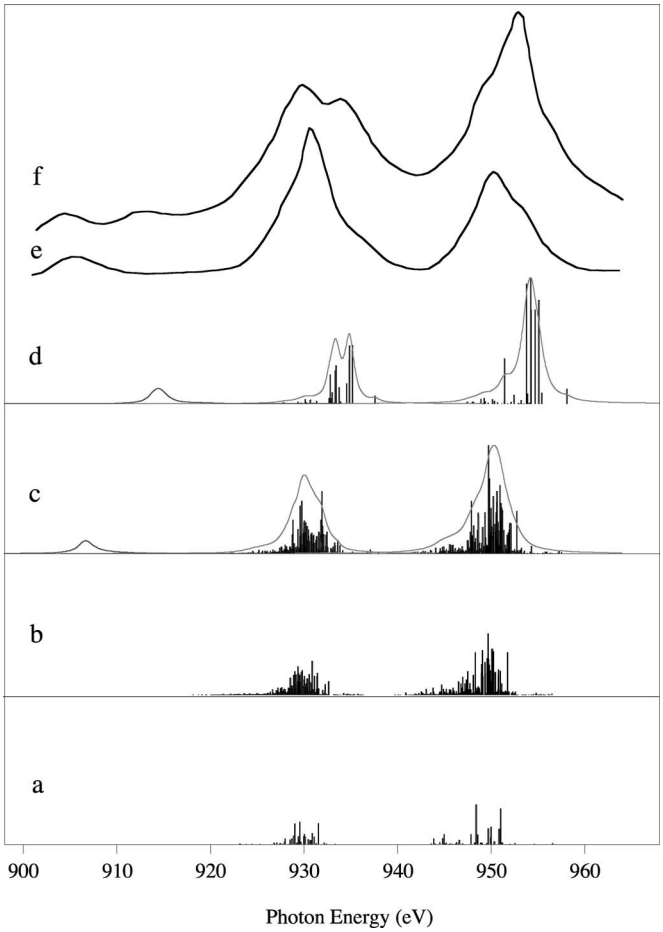

FIG. 3. Pr^{3+} calculated and experimental emissions: (a) resonance lines; (b) $J,J\pm1$ emissions; (c) $4f$-$3d$ and $5p$-$3d$ excitation emissions; (d) $4f$-$3d$ and $5p$-$3d$ ionization emissions; metal observed at (e) 1.1 and (f) 3.0 kV.

those in the oxide, contrary to what is known from the x-ray emission spectra. This led to the conclusion that, in our experiments, the excited states are created directly under electron bombardment.

The intensity of x-ray emissions depends on three factors: (a) the number of atom or ion in the initial state of the transition, here a state of the $3d^9 4f^{m+1}$ or $3d^9 4f^m$ configuration, (b) the transition probability normalized with the sum of the probabilities of all the possible decay processes, and (c) the self-absorption of the radiation in the target. The excitation cross section of an incident electron depends on the corresponding optical oscillator strength [11]. When the core hole is produced by incident electrons of energy E_0 close to the threshold energy, the excitation processes dominate; they decrease with increasing E_0. In contrast, the ionization cross sections that vanish at the threshold increase as $(E_0)^p$ (with $1.5 \leqslant p \leqslant 2$) [4], making the intensity of the diagram lines increases strongly with E_0. On the other hand, the self-absorption increases with E_0 and is maximum for the resonance lines and for the lines located at the same energy. As a result of the above processes, the relative intensities of the excitation and ionization emissions vary strongly with E_0. Such variation is observed and discussed below.

In what follows the rare earths will be divided into three groups: the light rare earths, the medium-weight rare earths around the half-filled $4f$ subshell, and the heavy rare earths. The experimental results are presented successively for these three groups. Some rare earths have several valences: they include Ce, Tm, and Yb as well as other rare earths around the middle of the series like Eu. Only the spectra of the trivalent rare earths are considered here.

A. The light rare earths: Ce, Pr, Nd

Cerium has two valences. The x-ray absorption spectrum of metallic Ce corresponds very closely to the multiplet structure of the $3d^9 4f^2$ configuration excited from the $3d^{10} 4f^1\ ^2F_{5/2}$ ground state [22,26]. This result confirms that Ce has three valence electrons in the metal. In contrast, the spectra of the Ce compounds generally correspond to a mixing of two valencies represented by the $3d^9 4f^2$ and $3d^9 4f^1$ configurations. They will not be considered here. The emission spectrum of metallic Ce, at E_0 equal to 1.5 keV, is plotted in Fig. 2 [27]. In order to fit the calculated and experimental spectra, the theoretical results had to be shifted by −2 eV. This value can supply an estimate of the shift due to the core-hole screening by the valence electrons. Each $3d_{5/2}$- and $3d_{3/2}$-based spectrum spreads over about 10 eV, in agreement with the calculations. The $3d_{5/2}$ main peak shows an unresolved feature, as expected from the calculated excitation emission. The feature observed toward the higher en-

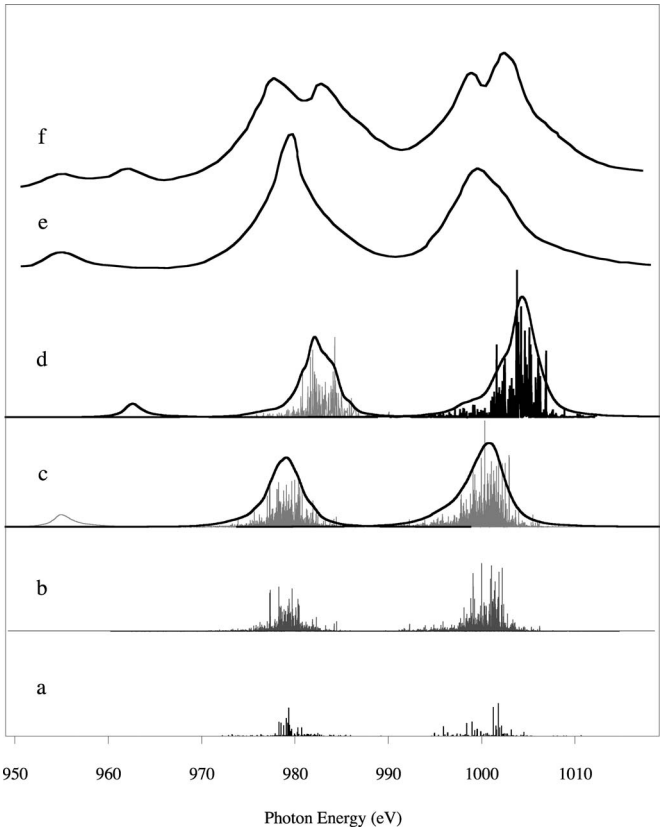

FIG. 4. Nd^{3+} calculated and experimental emissions: (a) resonance lines; (b) $J,J\pm1$ emissions; (c) $4f$-$3d$ and $5p$-$3d$ excitation emissions; (d) $4f$-$3d$ and $5p$-$3d$ ionization emissions; metal observed at (e) 1.2 and (f) 3.0 kV.

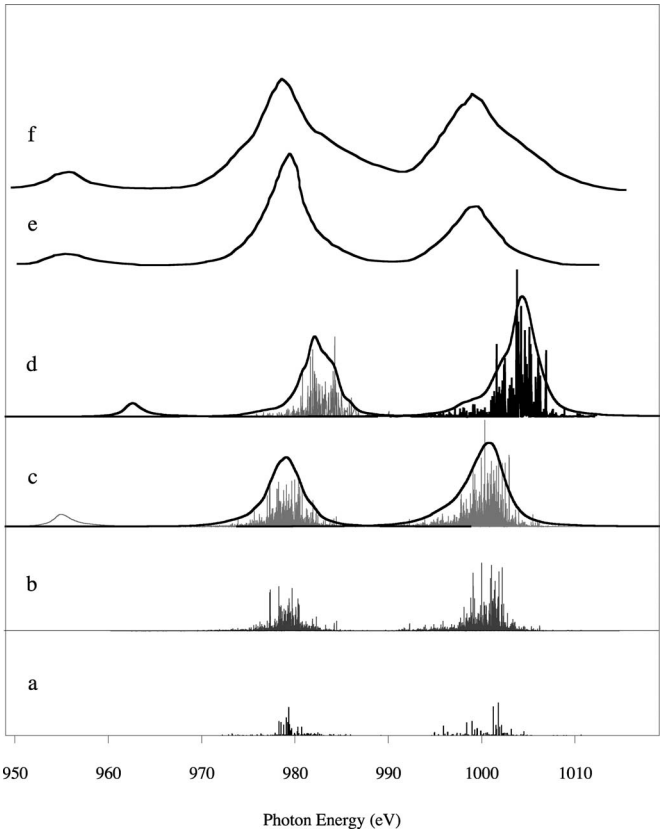

FIG. 5. Nd^{3+} calculated and experimental emissions: (a) resonance lines; (b) $J,J\pm1$ emissions; (c) $4f$-$3d$ and $5p$-$3d$ excitation emissions; (d) $4f$-$3d$ and $5p$-$3d$ ionization emissions; Nd_2O_3 observed at (e) 1.2 and (f) 3.0 kV.

ergies of the $3d_{5/2}$ spectrum corresponds to the $3d^9 4f^1\ ^3D_1 - 4f^0\ ^1S_0$ transition in the ion and that seen in the $3d_{3/2}$ spectrum to the $3d^9 4f^1\ ^1P_1 - 4f^0\ ^1S_0$ transition.

The Pr and Nd metal spectra are observed within an energy range that includes the $5p$-$3d_{5/2}$ transitions, at two different values of E_0. A comparison with calculated spectra is given in Figs. 3 and 4. The calculated spectra are shifted by -1 eV to take into account the screening by the valence electrons. The features located to the higher energies correspond to $4f$-$3d$ emissions in the ion, whose intensity increases with E_0. In contrast, the resonance lines excited at $E_0=3$ keV are strongly self-absorbed and their positions correspond to the minima clearly seen for Nd^{3+} and for the $3d_{5/2}$ range of Pr^{3+}. Toward the lower energies, the excitation emissions are in a range of weak self-absorption. At low values of E_0, the $5p$-$3d_{5/2}$ emission is observed only from the excited configuration. When E_0 increases, it is observed simultaneously from the excited and ionized configurations with similar intensities. The self-absorption is the same for the two emissions and also the $5p$-$3d$ radiative probabilities. Thus, at 3 keV, the excitation and ionization cross sections are approximatively the same for these elements.

The Nd^{3+} spectrum in the oxide is plotted in Fig. 5. Comparison between the two Nd^{3+} spectra clearly shows that they differ only by the relative intensities of the excitation and ionization emissions. As discussed above, in the metal, as a result of the tunneling of the $4f$ excited electrons, the population of the excited states decreases while that of the ionized states increases. The $4f$-$3d$ ionization emissions appear more intense than the excitation emissions at high E_0 energy. Inversely, for Nd^{3+} in the oxide, the intensity of the $4f$-$3d$ transitions is weak toward the higher energies, i.e., in the range of the ionization emissions, and the $5p$-$3d_{5/2}$ emission in the ion is not observed.

From our calculations, the $3d_{3/2}$ radiative transitions are expected to be more intense than the $3d_{5/2}$ transitions. The ionization emissions are induced by processes whose probabilities are in the ratio of the statistical weights. When the Pr and Nd $3d_{5/2}$:$3d_{3/2}$ ratios given Table II, column 4, are multiplied by the $3d_{5/2}$ and $3d_{3/2}$ weights, they remain smaller than unity, in agreement with the experiment. On the other hand, the Pr and Nd excitation emissions are observed following an excitation process. As already discussed, the number of excited states depends on the photoexcitation cross sections. The experimental and theoretical photoexcitations are clearly stronger in the $3d_{5/2}$ than the $3d_{3/2}$ range [22] and this explains why the experimental intensities of the excitation emissions are reversed with respect to the transition probabilities. Another parameter changes the $3d_{5/2}$:$3d_{3/2}$ ratio of the excitation emissions: the presence of resonant Coster-Kronig transitions of the $3d_{3/2}^{-1}4f^{m+1}$-$3d_{5/2}^{-1}4f^m$ type. As already mentioned, this parameter contributes to an increase in the experimental $3d_{5/2}$:$3d_{3/2}$ ratios of the excitation emissions with respect to the calculated ones.

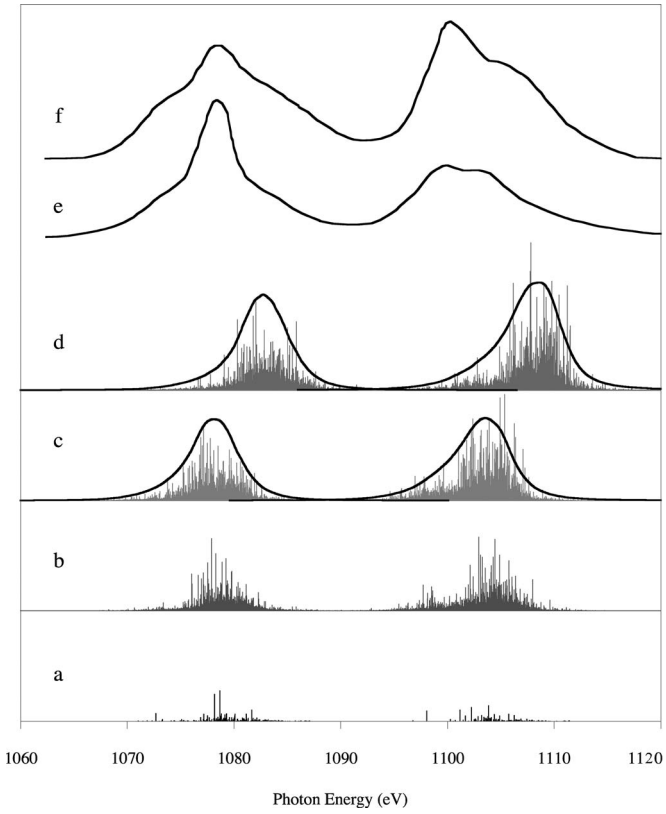

FIG. 6. Sm^{3+} calculated and experimental emissions: (a) resonance lines; (b) $J,J\pm1$ emissions; (c) $4f$-$3d$ excitation emissions; (d) $4f$-$3d$ ionization emissions; Sm_2O_3 observed at (e) 1.4 and (f) 3.0 kV.

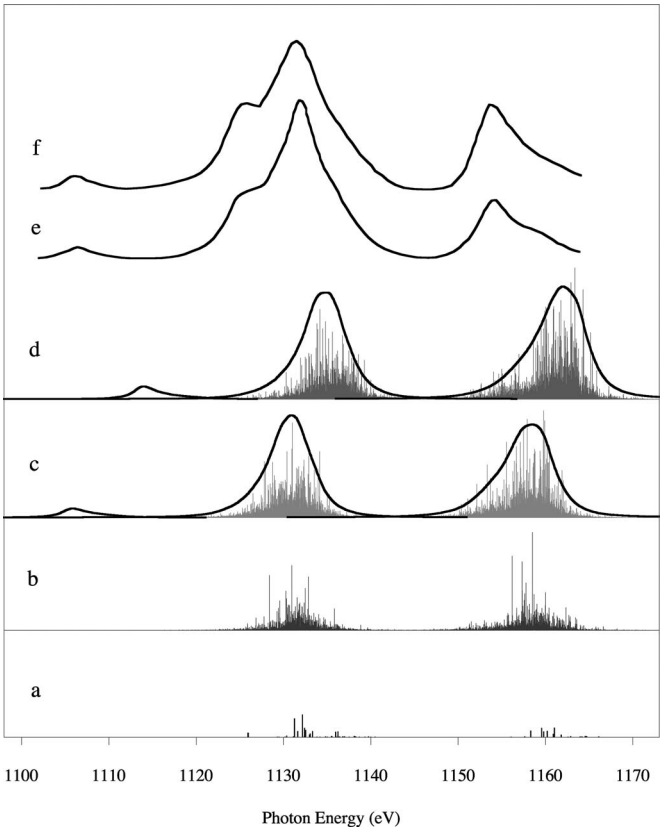

FIG. 7. Eu^{3+} calculated and experimental emissions: (a) resonance lines; (b) $J,J\pm1$ emissions; (c) $4f$-$3d$ and $5p$-$3d$ excitation emissions; (d) $4f$-$3d$ and $5p$-$3d$ ionization emissions; the $5p$-$3d$ emissions are multiplied by a factor 2. Eu_2O_3 observed at (e) 1.4 and (f) 2.3 kV.

B. Medium-weight rare earths: Sm, Eu, Gd, Tb

Europium is known to have two valences and to be divalent in the metal. Terbium generally presents several valence states in its compounds. Samarium too can have several valences. The spectra of Sm and Eu stable trivalent oxides and of Gd [3] and Tb metals are considered here.

The spectra of these elements are more complex than those of the light ones; they are spread out on a large energy range, particularly in the $3d_{3/2}$ region. For Sm, Eu, and Gd, the calculated spectra are shifted by −1 eV; for Tb, as for the heavy rare earths, no shift of the theoretical spectra is made. For Sm^{3+} (Fig. 6), in agreement with the calculations, the $3d_{5/2}$ and $3d_{3/2}$ excitation lines appear distributed in two parts, a lower-energy part, more spread for $3d_{3/2}$ than for $3d_{5/2}$, and a second part located in the energy range of the resonance lines. At low E_0 energy, the $3d_{5/2}$ excitation lines are more intense than the $3d_{3/2}$ ones because the $3d_{5/2}$ excitation cross sections, i.e., the numbers of $3d_{5/2}$ excited states, are larger than the $3d_{3/2}$ ones [22]. When E_0 exceeds twice the threshold, the $3d_{5/2}$:$3d_{3/2}$ ratio is reversed because the $3d_{5/2}$ self-absorption is very strong in the main part of the $3d_{5/2}$ emission while the main part of the $3d_{3/2}$ emission, located under the resonances lines, is in a region of weak self-absorption. The unresolved weak features located toward the higher energies correspond to the ionization emissions.

The same results are obtained for the three following elements (Figs. 7–9). The $5p$-$3d$ calculated intensities are multiplied by 2 with respect to the $4f$-$3d$ ones. For Eu^{3+}, as for Nd^{3+} oxide (Fig. 5), the $5p$-$3d$ emission in the ionized state is not observed and the features of higher energies have very weak intensities. The number of ionized states created at 2.3 keV is small with respect to the number of excited states. In contrast, for Gd^{3+} metal, as for Nd^{3+} metal (Fig. 4), the $5p$-$3d$ emission in the ionized state and the higher-energy features are clearly observed and their intensity increases with the E_0 energy. At high values of E_0, the intensity decreases at the position of the resonance lines and, by contrast, seems to increase strongly in the energy range located under the resonance lines, making them appear the equivalent of peaks. For the three elements, at low E_0 energy, the intensity is higher in the $3d_{5/2}$ than the $3d_{3/2}$ range because the excitation probability is larger in the $3d_{5/2}$ range. At high E_0 energy, the $3d_{3/2}$ low-energy peaks are more important than the $3d_{5/2}$ ones because they are located under the absorption lines and weakly self-absorbed while the self-absorption is very strong in the $3d_{5/2}$ range.

An example of the spectral changes with the E_0 incident energy is presented in Fig. 10 for Sm^{3+}. The relative intensity of the excitation emissions with respect to the ionization emissions decreases when E_0 increases. At 5 keV, the $3d_{5/2}$ absorption lines located around 1080 eV strongly change the shape of the $3d_{5/2}$ spectrum and are responsible for the reverse of the intensities with respect to the 3 keV spectrum.

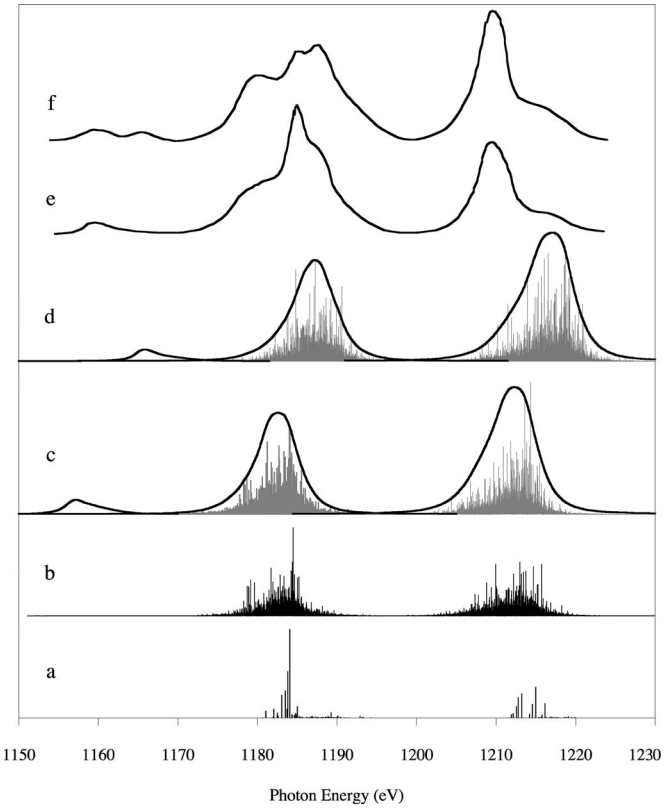

FIG. 8. Gd^{3+} calculated and experimental emissions: (a) resonance lines; (b) $J,J\pm1$ emissions; (c) 4*f*-3*d* and 5*p*-3*d* excitation emissions; (d) 4*f*-3*d* and 5*p*-3*d* ionization emissions; the 5*p*-3*d* emissions are multiplied by a factor 2. Metal observed at (e) 1.4 and (f) 2.25 kV.

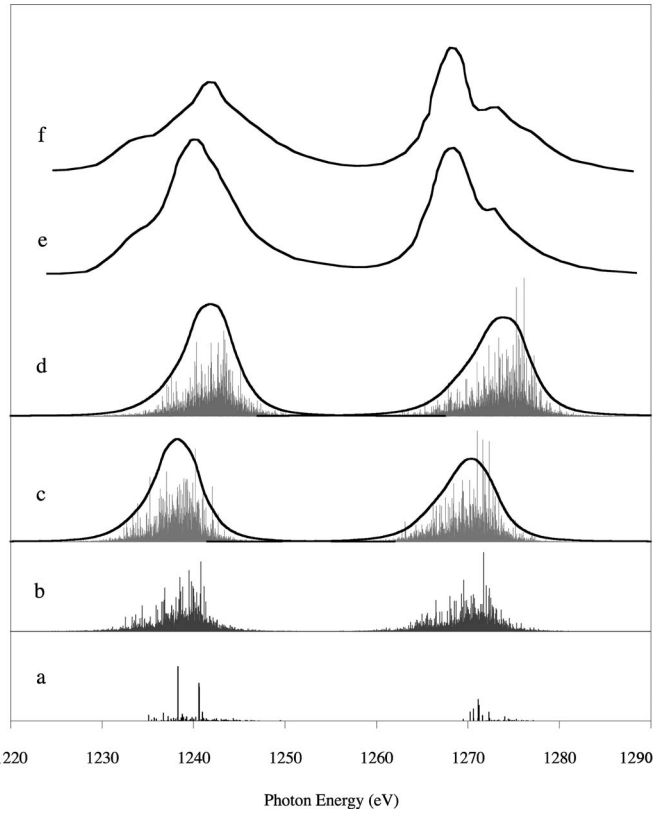

FIG. 9. Tb^{3+} calculated and experimental emissions: (a) resonance lines; (b) $J,J\pm$ emissions; (c) 4*f*-3*d* excitation emissions; (d) 4*f*-3*d* ionization emissions; metal observed at (e) 1.4 and (f) 3.0 kV.

No $3d_{3/2}$ absorption line is located below 1102 eV and the excitation emission has a relatively large intensity in this energy range. Let us consider the case where E_0 is very near the threshold and equal to 1140 eV. The Sm $3d_{5/2}$ and $3d_{3/2}$ thresholds are, respectively, 1080 and 1106 eV. While E_0 exceeds the $3d_{5/2}$ threshold by 60 eV, the difference is only 30 eV for the $3d_{3/2}$ threshold. As a consequence of secondary effects, depending on the interactions of the incident electrons with the target, the $3d_{5/2}$:$3d_{3/2}$ emission ratio observed at such a low E_0 energy does not correspond to the real value and must not be taken into account.

C. Heavy rare earths: Dy, Ho, Er, Tm, Yb

Ytterbium has two valences; it is trivalent in the compounds and divalent in the metal. Thullium, generally trivalent, has two and three valences in some compounds. The spectra of the trivalent oxide are considered for the five elements.

For the heavy rare earths, the $3d_{3/2}$ resonance line probabilities decrease progressively and no $3d_{3/2}$ resonance line is expected for Yb^{3+}. One $3d_{3/2}$ weak resonance line is expected for Tm^{3+}. The distance between the excitation and ionization emissions decreases, making the resolution of the two types of transitions difficult. As for the previous elements, the $3d_{3/2}$ resonance lines are located toward the higher energies of the excitation spectrum and only this range is self-absorbed. The $3d_{5/2}$ resonance lines are spread on an energy range wider than that of the $3d_{3/2}$ resonance lines. For Dy^{3+} and Ho^{3+} (Figs. 11 and 12), the number of lines is large and the ionization emissions appear only as tails toward the higher energies. The characteristics of the spectra gradually change in the same manner as for the previous elements except that no reverse of the $3d_{5/2}$ and $3d_{3/2}$ intensities is observed with increasing E_0. For Dy^{3+}, a weak 5*p*-3*d* emission in the presence of the 4*f* spectator electron is observed. In Fig. 11, the 5*p*-3*d* calculated intensities are multiplied by 4 with respect to the 4*f*-3*d* intensity. For the other elements, the 5*p*-3*d* emissions are too weak to be given simultaneously with the 4*f*-3*d* emissions.

Erbium is the first element whose calculated $3d_{5/2}$:$3d_{3/2}$ ratio is different for the $J,J\pm1$ emissions and for the excitation emissions (Table II). This difference increases strongly for Tm^{3+}. However no rapid change of the spectral characters is observed for these two elements with respect to previous ones (Figs. 13 and 14). This suggests that the experimental spectra correspond to the excitation emissions.

For the three last elements, the number of lines decreases. However, the excitation and ionization emissions are unresolved because the distance between them decreases continuously along the series. For Yb^{3+} in the $3d_{5/2}$ range, the strongest line of the $J,J\pm1$ and excitation emissions is expected toward the lower energies of the ionization lines. It is clearly

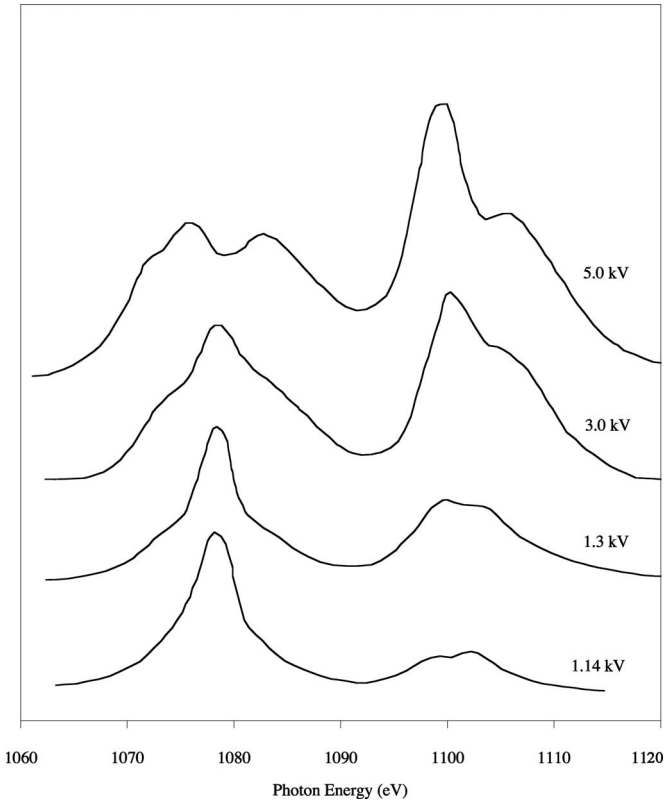

FIG. 10. Sm_2O_3 observed at 1.14, 1.5, 3.0, and 5.0 kV.

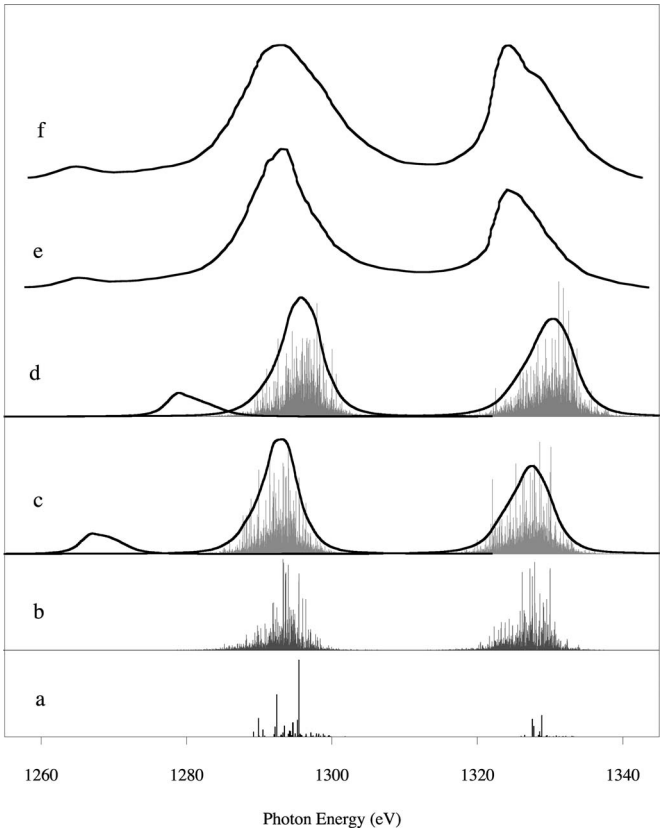

FIG. 11. Dy^{3+} calculated and experimental emissions: (a) resonance lines; (b) $J,J\pm1$ emissions; (c) $4f$-$3d$ and $5p$-$3d$ excitation emissions; (d) $4f$-$3d$ and $5p$-$3d$ ionization emissions; the $5p$-$3d$ emissions are multiplied by a factor 4. Dy_2O_3 observed at (e) 1.5 and (f) 2.8 kV.

observed (Fig. 15). In the $3d_{3/2}$ range, no $J,J\pm1$ emission and one excitation line is expected. This line is approximately at the same energy as one of the ionization lines and its presence in the spectrum is not definitely established. Thus for Yb^{3+}, it is difficult to say if the observed spectrum corresponds to the excitation emissions or to $J,J\pm1$ emissions.

V. DISCUSSION

The E_0 energy of the incident electron beam is an important experimental parameter because it governs the spectral intensities and can strongly modify them. One of the advantages of the electron impact excitation is to control the self-absorption and thereby to reduce it to a minimum. This is important for the $3d$ rare-earth emissions because the self-absorption can eclipse the resonance lines.

From the relative intensity of the well-resolved $5p$-$3d_{5/2}$ emissions, we have estimated the relative abundances of the excited and ionized configurations created under electron bombardment in our experimental conditions. The probability of ionization processes is small at low E_0 energies and approximately the same as that of excitation processes when E_0 is of the order of twice the threshold. This result is valid only for the spectra of a nonconductor compound. In the case of a conductor, attention must be given to mixing between the discrete and extended states because they contribute to decreasing the number of excited states.

The $4f$-$3d$ emissions of the rare earths are interpreted using calculations based on the MCDF method including Breit and QED terms. The features observed toward the higher energies of the $3d$ resonance lines, i.e., of the $3d$ photoexcitation lines, are identified as the $4f$-$3d$ ionization emissions while those located toward the lower energies are attributed to $4f$-$3d$ excitation emissions. This interpretation is in agreement with the observation of both $5p$-$3d$ diagram emissions and $5p$-$3d$ emissions in the presence of a spectator $4f$ electron. The spectral characteristics that are observed to change gradually along the series are well reproduced by the theoretical calculations as indicated in Tables I–III.

The particularities of the rare-earth $3d$ emission spectra are governed by important parameters already discussed above: the highly localized nature of the $4f$ states; the large energy extension of the excited and ionized configurations, making the emissions widely spread and unchanged by the broadening due to the level lifetime; the strong self-absorption associated with the $4f$-$3d$ resonance lines, introducing a large distortion of the spectra.

Another important problem is the population of the excited states. Electron excitation populates all the J levels of the excited configurations. However, as already underlined, the levels accessible by dipolar selection rules from the ground state are excited preferentially. The role of the dipole selection rules increases with the incident electron energy E_0. For E_0 of the order of 1.5 times the threshold energy, the excitation process is totally governed by these rules. Thus the

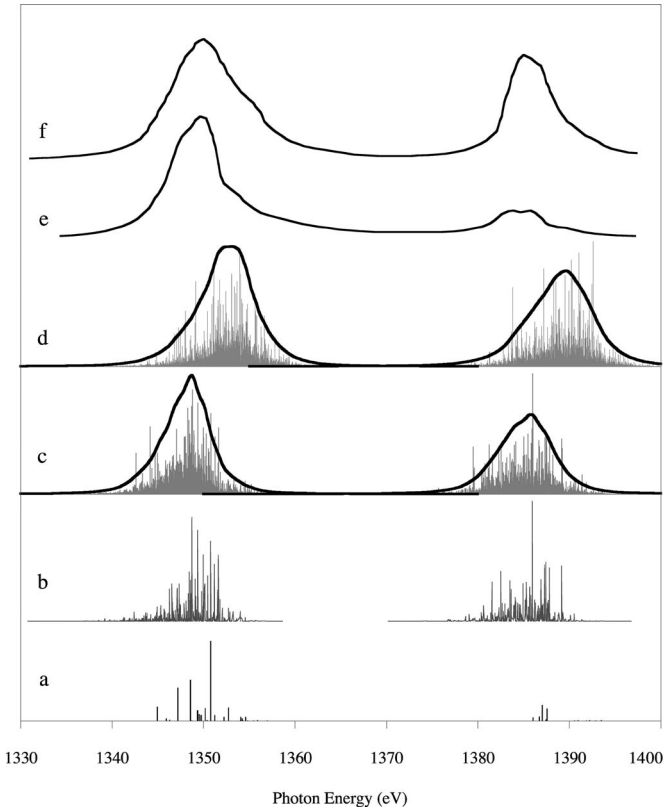

FIG. 12. Ho^{3+} calculated and experimental emissions: (a) resonance lines; (b) $J,J\pm$ emissions; (c) 4*f*-3*d* excitation emissions; (d) 4*f*-3*d* ionization emissions; Ho_2O_3 observed at (e) 1.5 and (f) 2.8 kV.

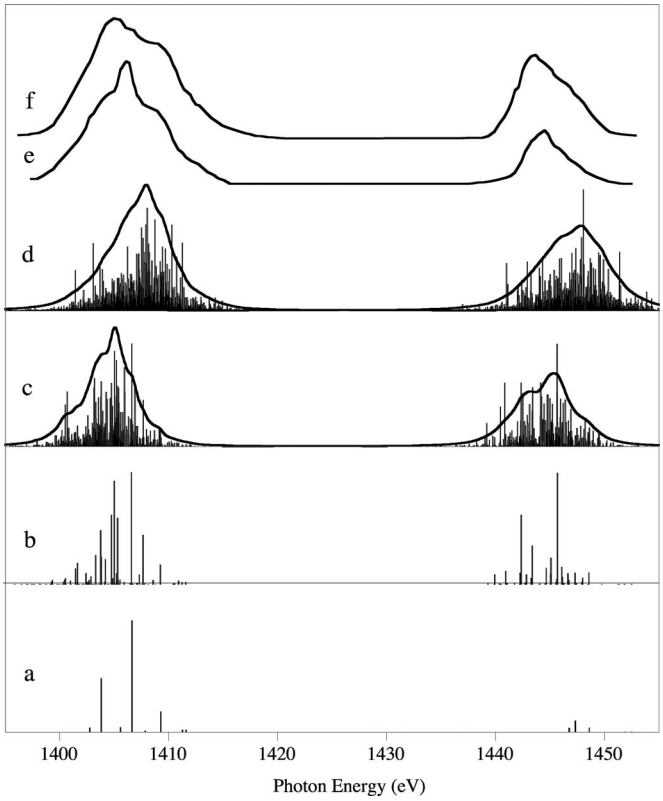

FIG. 13. Er^{3+} calculated and experimental emissions: (a) resonance lines; (b) $J,J\pm1$ emissions; (c) 4*f*-3*d* excitation emissions; (d) 4*f*-3*d* ionization emissions; Er_2O_3 observed at (e) 1.6 and (f) 2.4 kV.

initial population of the excited configuration depends on the excitation conditions.

Redistribution of these selectively excited levels among all the J levels of the excited configuration leads to their statistical population. Such a statistical reorganization assures that both radiative and nonradiative decay processes take place independently and are two-step processes. The relative intensities of the 4*f*-3*d* and 5*p*-3*d* emissions are, thus, in the ratio of the corresponding transition probabilities. On the other hand, if the recombination of the 4*f* excited electron to the inner hole takes place more rapidly than the statistical reorganization, only the radiative transitions from the excited $J,J\pm1$ states and the nonradiative resonant transitions from the same states should be observed.

The energy distribution of the incident electron beam is spread over some eV and the interaction of the electron beam with the system is more rapid than the decay of the 3*d* core hole. The time scale of the statistical reorganization of the J levels is shorter than the average lifetime of each J level. All the J levels of the excited and ionized configurations are already statistically populated when the slow decay processes, such as the 5*p*-3*d* emissions, start to take place and contribute to the emission spectra.

The observed relative intensities of the 4*f*-3*d* and 5*p*-3*d* emissions are in good agrement with the calculated transition probabilities. This shows that both emissions take place from the same configuration, i.e., after the statistical reorganization. Moreover, the $3d_{5/2}:3d_{3/2}$ ratio changes gradually across the entire series as expected for excitation emissions. We conclude that all the J levels of the $3d^9 4f^{m+1}$ excited configurations are statistically populated before the radiative decay. The same behavior is expected for the $3d^9 4f^m$ ionized configurations. We have shown that the *d*-*f* electrostatic interactions between the different J levels of a ion with a 3*d* hole govern its spectral characteristics, such as the $3d_{5/2}:3d_{3/2}$ ratio. These interactions also govern the population of the J levels of the excited and ionized configurations. The same criteria apply in the case of the 4*d* spectra [14].

VI. CONCLUSION

A general free-ion model using a MCDF program including Breit terms is applied for the interpretation of the 4*f*-3*d* emission spectra induced by electron impact in the trivalent rare-earth series. A very good agreement is obtained between the calculations and the observed features for the solid. The 4*f*-3*d* and 5*p*-3*d* transitions are observed at the same energies for the metal and the oxide as long as the valence of the rare earth remains the same. These transitions are thus independent of the chemical surroundings. This confirms that interactions between the localized 4*f* electrons and the valence bands can be neglected and justifies the use of an atomic model to describe the 4*f* core-level transitions. The valence electrons introduce only a screening whose effect is to re-

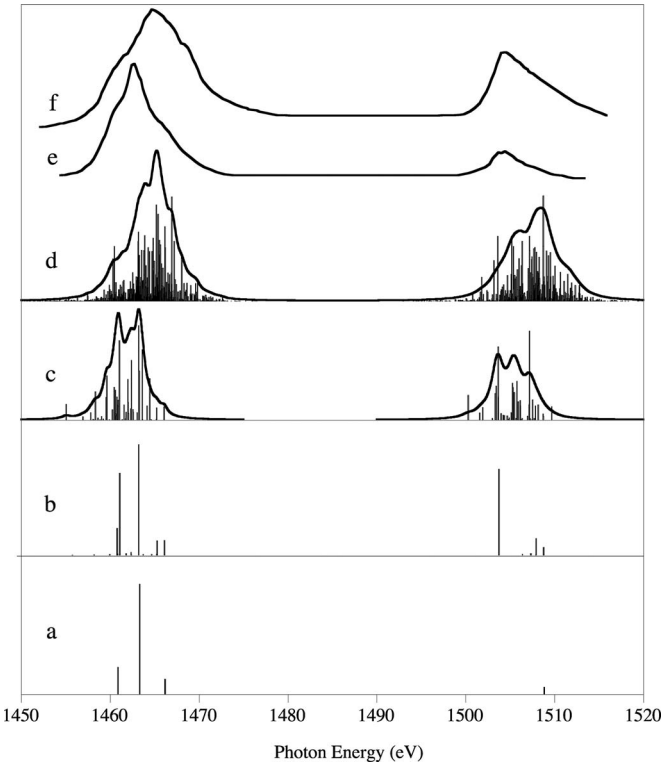

FIG. 14. Tm^{3+} calculated and experimental emissions: (a) resonance lines; (b) $J,J\pm$ emissions; (c) $4f$-$3d$ excitation emissions; (d) $4f$-$3d$ ionization emissions; Tm_2O_3 observed at (e) 1.6 and (f) 3.0 kV.

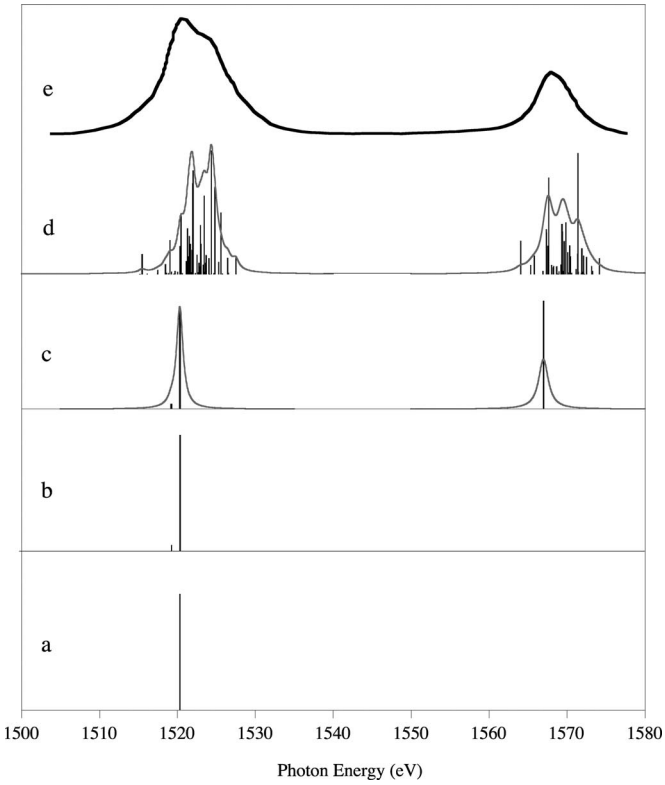

FIG. 15. Yb^{3+} calculated and experimental emissions: (a) resonance lines; (b) $J,J\pm1$ emissions; (c) $4f$-$3d$ excitation emissions; (d) $4f$-$3d$ ionization emissions; Yb_2O_3 observed at (e) 1.7 and (f) 3.0 kV.

duce the level energies. This effect is represented by the slight difference between calculated and experimental energies and noticeable only for the light rare earths.

The intensity ratios observed for the $4f$-$3d_{5/2}$ and $4f$-$3d_{3/2}$ emissions and for the $4f$-$3d$ and $5p$-$3d$ ones are in good agreement with calculations that take into account all the multiplet states of the various configurations. General information on the dynamics of the excited and ionized states with a $3d$ hole is discussed. We conclude that all the levels of the excited and ionized configurations are statistically populated prior to their decay. This is a systematic behavior along the lanthanide series. Relative probabilities to create the various possible initial states are estimated as a function of the incident electron energy. Our study shows that the essential characteristics of the $3d$ spectra of the trivalent rare earths are due to the $3d$-$4f$ Coulomb interaction and this underlines the dominant role played by this interaction in the nd spectra of atoms or ions with an open f subshell.

ACKNOWLEDGMENTS

The authors wish to thank Dr. N. Spector for his enlightening remarks concerning the manuscript and Dr. P. Jonnard for his assistance in the treatment of the experimental data. They acknowledge the Centre de Calcul Recherche et Enseignement de l'Université Pierre et Marie Curie for computer facilities.

[1] E. A. Stewardson and J. E. Wilson, Proc. Phys. Soc., London, Sect. A **69**, 93 (1956).
[2] D. W. Fischer and W. L. Baun, J. Appl. Phys. **38**, 4830 (1967).
[3] C. Bonnelle and R. C. Karnatak, C.R. Seances Acad. Sci., Ser. A **268**, 494 (1969); J. Phys. (Paris), Colloq. **32**, C4-230 (1971).
[4] C. Bonnelle, Annual Report C, Royal Society of Chemistry, London, 1987, p. 201.
[5] R. E. LaVilla, Phys. Rev. A **9**, 1801 (1974).
[6] M. Okusawa, K. Ichikawa, O. Aita, and K. Tsutsumi, Phys. Rev. B **35**, 478 (1987).
[7] M. Pompa, A. M. Flank, P. Lagarde, J. C. Rife, I. Stekhin, M. Nakazawa, H. Ogasawara, and A. Kotani, Phys. Rev. B **56**, 2267 (1997).
[8] S. M. Butorin, L.-C. Duda, J.-H. Guo, N. Wassdah, J. Nordgren, M. Nakazawa, and A. Kotani, J. Phys.: Condens. Matter **9**, 8155 (1997).
[9] A. Moewes, S. Stadler, R. P. Winarski, D. L. Ederer, M. M. Grush, and T. A. Callcott, Phys. Rev. B **58**, R15951 (1998).
[10] A. Moewes, D. L. Ederer, M. M. Grush, and T. A. Callcott,

Phys. Rev. B **59**, 5452 (1999).
[11] N. F. Mott and H. S. W. Massey, *The Theory of Atomic Collisions* (Clarendon Press, Oxford, 1965).
[12] F. P. Netzer, G. Strasser, and J. A. D. Matthew, Phys. Rev. Lett. **51**, 211 (1983).
[13] G. Strasser, G. Rosina, J. A. D. Matthew, and F. P. Netzer, J. Phys. F: Met. Phys. **15**, 739 (1985).
[14] C. Bonnelle, G. Giorgi, and J. Bruneau, Phys. Rev. B **50**, 16255 (1994).
[15] C. Bonnelle, P. Jonnard, C. Barré, G. Giorgi, and J. Bruneau, Phys. Rev. A **55**, 3422 (1997).
[16] J. Bruneau, J. Phys. B **16**, 4135 (1983).
[17] S. J. Rose, N. D. C. Pyper, and I. P. Grant, J. Phys. B **11**, 755 (1978).
[18] R. D. Deslattes, E. G. Kessler, P. Indelicato, L. de Billy, E. Lindroth, and J. Anton, Rev. Mod. Phys. **75**, 35 (2003).
[19] M. H. Chen, B. Crasemann, and H. Mark, Phys. Rev. A **21**, 449 (1980).
[20] P. Motais, E. Belin, and C. Bonnelle, Phys. Rev. B **30**, 4399 (1984).
[21] E. J. McGuire, Phys. Rev. A **5**, 1043 (1972).
[22] B. T. Thole, G. van der Laan, J. C. Fuggle, G. A. Sawatzky, R. C. Karnatak, and J.-M. Esteva, Phys. Rev. B **32**, 5107 (1985).
[23] J. A. Bearden and A. F. Burr, Rev. Mod. Phys. **39**, 125 (1967).
[24] J. C. Fuggle, M. Campagna, Z. Zolnierek, R. Lasser, and A. Platau, Phys. Rev. Lett. **45**, 1597 (1980).
[25] M. Ohno, J. Electron Spectrosc. Relat. Phenom. **143**, 9 (2005).
[26] C. Bonnelle, R. C. Karnatak, and J. Sugar, Phys. Rev. A **9**, 1920 (1974).
[27] A. Sonder, Ph.D. thesis, Université Pierre et Marie Curie, Paris, 1991 (unpublished).